Near-Infrared Plasmonic-Enhanced Solar Energy Harvest for Highly Efficient Photocatalytic Reactions

ARTICLE *in* NANO LETTERS · SEPTEMBER 2015

Impact Factor: 13.59 · DOI: 10.1021/acs.nanolett.5b00950

NANO LETTERS

Letter

pubs.acs.org/NanoLett

Near-Infrared Plasmonic-Enhanced Solar Energy Harvest for Highly Efficient Photocatalytic Reactions

Jiabin Cui,[†] Yongjia Li,[‡] Lei Liu,[§] Lin Chen,[†] Jun Xu,[†] Jingwen Ma,[†] Gang Fang,[†] Enbo Zhu,[‡] Hao Wu,[‡] Lixia Zhao,[§] Leyu Wang,*[,†] and Yu Huang*[,‡]

[†]State Key Laboratory of Chemical Resource Engineering, Beijing University of Chemical Technology, Beijing 100029, People's Republic of China

[‡]Department of Materials Science and Engineering, University of California Los Angeles, Los Angeles, California 90095 United States

[§]Semiconductor Lighting Technology Research and Development Center, Institute of Semiconductors, Chinese Academy of Sciences, Beijing 100083, People's Republic of China

Supporting Information

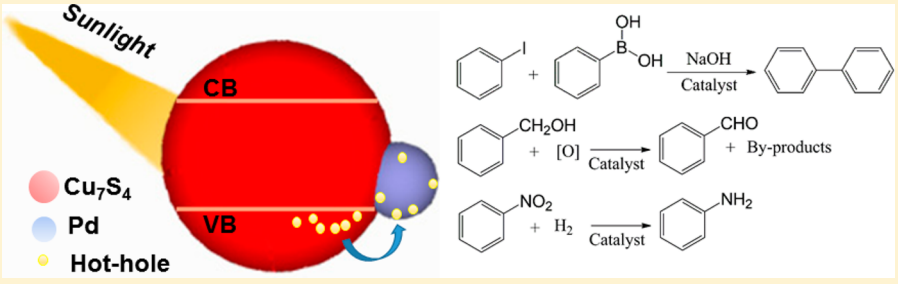

ABSTRACT: We report a highly efficient photocatalyst comprised of Cu_7S_4@Pd heteronanostructures with plasmonic absorption in the near-infrared (NIR)-range. Our results indicated that the strong NIR plasmonic absorption of Cu_7S_4@Pd facilitated hot carrier transfer from Cu_7S_4 to Pd, which subsequently promoted the catalytic reactions on Pd metallic surface. We confirmed such enhancement mechanism could effectively boost the sunlight utilization in a wide range of photocatalytic reactions, including the Suzuki coupling reaction, hydrogenation of nitrobenzene, and oxidation of benzyl alcohol. Even under irradiation at 1500 nm with low power density (0.45 W/cm^2), these heteronanostructures demonstrated excellent catalytic activities. Under solar illumination with power density as low as 40 mW/cm^2, nearly 80−100% of conversion was achieved within 2 h for all three types of organic reactions. Furthermore, recycling experiments showed the Cu_7S_4@Pd were stable and could retain their structures and high activity after five cycles. The reported synthetic protocol can be easily extended to other Cu_7S_4@M (M = Pt, Ag, Au) catalysts, offering a new solution to design and fabricate highly effective photocatalysts with broad material choices for efficient conversion of solar energy to chemical energy in an environmentally friendly manner.

KEYWORDS: *Heteronanostructures, solar photocatalysis, localized surface plasmon resonances (LSPR), copper sulfide*

The direct conversion of solar energy to chemical energy using photocatalysts has received significant attention. Up to now, semiconductor−semiconductor, semiconductor−metal, and bimetal heteronanostructures have emerged as promising photocatalysts for photodegradation of organic contaminants,[1−3] hydrogen generation,[4−8] conversion of CO_2,[9] and organic synthetic reactions.[10−12] For example, palladium-based nanostructures have been widely employed for the catalytic reaction including the hydrogenation of nitrobenzene, oxidation of benzyl alcohol, and Suzuki coupling reaction due to their excellent catalytic activity.[7,10,11,13,14] In order to enhance the catalytic activity and reduce the dosage of noble metal, a number of synthetic strategies have been developed to fabricate nanostructures with open surface features such as desired active facets,[15−17] porous structures,[11,12] concave surfaces,[18−20] and nanoframe structures with small sizes.[21−23] In terms of photocatalyst design, more and more research efforts have been given to improve direct utilization of sunlight in the visible region.[24−26] In addition, to enhance the light conversion efficiency, localized surface plasmon resonances (LSPR), arising from the collective oscillation of free carriers in the individual nanostructure stimulated by incident light, has been widely modeled and explored in noble metal nanostructures[5,27−31] for plasmonic photocatalysis,[10,13,25,27,28,32] sensors,[31,33,34] and photothermal ablation[35,36] applications.

Although noble metal nanostructure can be used alone as LSPR component and catalyst,[25−27] the semiconductor−metal heteronanostructures are relatively cheap and can offer higher light harvesting efficiency. To date, CeO_2−Au,[37] Cu_2O−Au,[38] TiO_2−Au,[39] CeO_2−Pt,[40] and CdS-Pt[41] heteronanostructures have been developed for photocatalytic H_2 generation. ZnO-

Received: March 10, 2015
Revised: August 23, 2015
Published: September 7, 2015

DOI: 10.1021/acs.nanolett.5b00950
Nano Lett. 2015, 15, 6295−6301

Au,[42] Cu_2ZnSnS_4–Pt[6] and Cu_2O–Au[43] heteronanostructures have been utilized for photodegradation of organic pollutants. All of them mainly make use of the visible or ultraviolet range irradiation light as energy source. According to the energy distribution in the solar spectrum, around 54.3%, 38.9%, and 6.8% of sunlight at the earth's surface is located in the near-infrared (NIR, 760–3000 nm), visible (vis, 400–760 nm), and ultraviolet (UV, <400 nm) range, respectively.[44] Therefore, the development of semiconductor–noble metal heteronanostructures with NIR absorption, low cost, high stability, and outstanding catalytic performance is still critical and highly desirable for efficient solar photosynthesis. The copper chalcogenide nanocrystals demonstrating excellent tunable plasmonic absorption especially in the NIR region are promising candidates for building plasmon enhanced photocatalysts. Besides, their potential as organic reaction catalysts has not yet been fully explored.[45−49]

Herein, for the first time we report a facile wet-chemistry strategy to synthesize heteronanostructure photocatalyst containing both noble metal (Pd) and Cu_7S_4 domains with intimate interfacial contact. These Cu_7S_4@Pd nanocrystals, by combining NIR LSPR light-harvesting property of Cu_7S_4 with the catalytic features of Pd, are excellent catalysts for solar photocatalysis of organic synthesis reactions. The LSPR effect enhanced photocatalytic activities of the Cu_7S_4@Pd heteronanostructures have been confirmed by both simulation studies and experimental evaluations through a series of organic reactions including Suzuki coupling reaction, selective oxidation of benzyl alcohol, and hydrogenation of nitrobenzene.

In a typical synthesis, Cu_7S_4 nanocrystals were prepared by solvothermal decomposition of the single precursor $Cu(S_2CNBut_2)_2$ containing both copper and sulfur dissolved in oleylamine.[50] The synthesis of Cu_7S_4@Pd was accomplished following a typical hot-injection method by introducing noble metal precursor $Pd(S_2CNBut_2)_2$ into the as-prepared Cu_7S_4 colloids. All synthetic steps were carried out under air-free conditions (see Supporting Information for details). Figure 1 shows the transmission electron microscopy (TEM) image and high-resolution transmission electron microscopy (HRTEM) image of Cu_7S_4@Pd. The average size of Cu_7S_4 is 14 nm and the size of Pd particles grown onside is 4.3 nm. For each Cu_7S_4 nanoparticle, more than one Pd particle can be found attached to the surface. The HRTEM image (Figure 1b) demonstrates an interplanar distance of 0.193 nm in semiconductor domain, consistent with the (0 16 0) lattice spacing of anilite Cu_7S_4. In the noble metal domains, an interplanar distance of 0.224 nm indicates the face-centered cubic (fcc) Pd (111) planes. HRTEM results also reveal the intimate metal–semiconductor interface in the heteronanostructure, which is highly favorable for charge transfer in between.[51] In comparison, TEM images of Cu_7S_4 nanoparticles and Pd nanoparticles are shown in Supporting Information Figure S1. The crystallinity of the semiconductor domains and noble metal domains was further examined through powder X-ray diffraction (XRD) patterns (Figure 1c). The two distinct sets of diffraction peaks can be assigned to the anilite Cu_7S_4 (JCPDS card 23-0958, Supporting Information Table S1) and Pd (JCPDS card 46-1043), respectively. Therefore, both TEM images and XRD patterns confirm the successful synthesis of the desired heteronanostructures. Furthermore, other heteronanostructures including Cu_7S_4@Au, Cu_7S_4@Pt, and Cu_7S_4@Ag can be prepared following similar procedures (see Supporting Information for details). By analyzing XRD patterns and HRTEM images, we also verified those heteronanostructures are composed of anilite Cu_7S_4 and noble metal components with good crystallinity and tight interfacial connection (Supporting Information Figures S2 and S3).

The LSPR absorption spectra of Cu_7S_4@Pd, Cu_7S_4, and Pd were measured experimentally (Figure 2a) and simulated by finite difference time domain (FDTD) method (Figure 2b). Pd

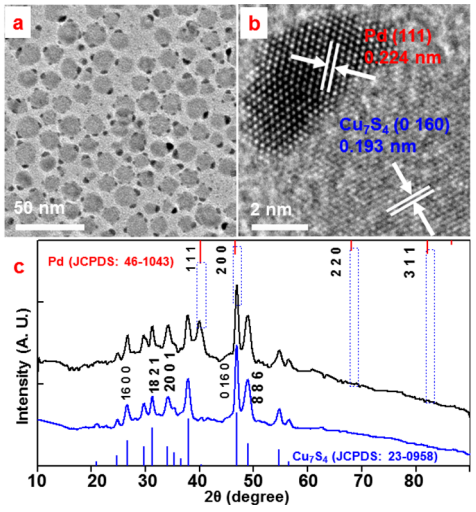

Figure 1. (a) TEM and (b) HRTEM images of Cu_7S_4@Pd. (c) XRD patterns of Cu_7S_4@Pd (black curve) and Cu_7S_4 (blue curve).

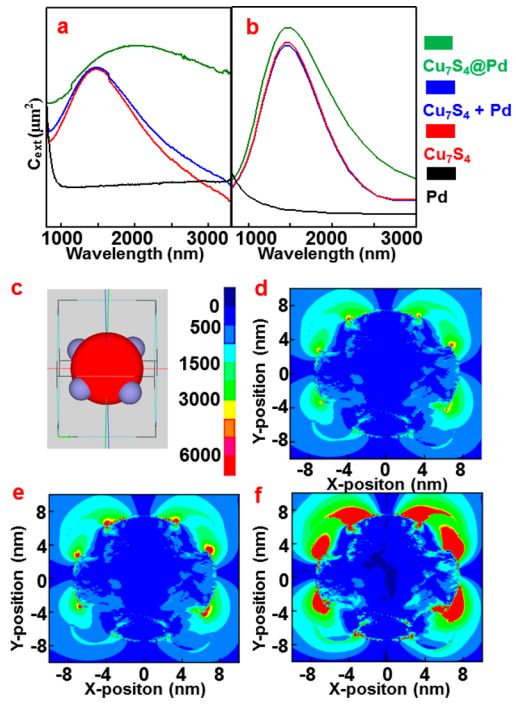

Figure 2. LSPR absorption spectra of different nanostructures obtained from experiment (a) and FDTD simulation (b). Green curves: Cu_7S_4@Pd heteronanostructures. Blue curves: physical mixture of Cu_7S_4 and Pd nanoparticles. Red curves: Cu_7S_4 nanoparticles. Black curves: Pd nanoparticles. (c) FDTD simulation setup for Cu_7S_4@Pd and electrical field intensity scale. (d–f) The 2D contour of the electric field intensities around the Cu_7S_4@Pd heteronanostructures under illumination of 808 nm (d), 980 nm (e), and 1500 nm (f), respectively.

DOI: 10.1021/acs.nanolett.5b00950
Nano Lett. 2015, 15, 6295–6301

demonstrates no LSPR peak above 1000 nm, while pure Cu_7S_4 or physical mixture of Cu_7S_4 and Pd gives clear absorption peak around 1500 nm, which can be observed from simulation as well. Moreover, the Cu_7S_4@Pd heteronanostructure demonstrates a red shift (~500 nm from experimental result) in LSPR peak with respect to that of Cu_7S_4. It has been reported that LSPR intensity in Cu_7S_4 heavily relies on free carrier density in the form of cation deficiencies.[52] Pd growth on Cu_7S_4 surface can possibly bond with sulfur atoms and reduce the exposure of Cu_7S_4 to oxygen, which might annihilate vacancies in Cu_7S_4, resulting in LSPR peak red shift.[52] We may also relate the red shift to the refractive index change originated from the incorporation of Pd to LSPR surface, as observed by other groups.[53,54] Additionally, peak broadening effect of heteronanostructures were observed in both experimental and simulation results with reference to pure Cu_7S_4 and the mixture of Cu_7S_4 and Pd. Again it can be attributed to the larger dielectric constant of Pd compared to that of the solvent.[52−55] We also note the experimental spectrum of the Cu_7S_4@Pd heteronanostructures differs from the FDTD simulation spectrum in terms of peak position and peak width. We postulate this difference as a result of the inhomogeneous structure and size distribution of the real heteronanostructure sample, similar to previously reported phenomena.[56−61]

LSPR effect is generally believed to be manifested in local electrical field enhancement.[46] To demonstrate the presence of this enhancement spatially and study its correlation with various wavelengths, the two-dimensional (2D) contour of the electron field intensity (XOY-plane, z = 0 nm) by FDTD simulation with illumination source of 808 (Figure 2d), 980 (Figure 2e), and 1500 nm (Figure 2f) are demonstrated by locating the Cu_7S_4@Pd nanocrystal in the center of a simulated box (Figure 2c). Control trials on Pd and Cu_7S_4 were also performed (Supporting Information Figures S4 and S5). Very weak LSPR feature was observed around the Pd nanoparticle at 808, 980, and 1500 nm irradiation (Supporting Information Figure S4). Pd nanoparticles themselves barely have LSPR absorption at these three wavelengths and thus are unlikely the source of LSPR enhancement. Meanwhile, Cu_7S_4 exhibits significant electrical field enhancement (Supporting Information Figure S5) with 1500 nm source triumphs other two wavelengths. Consequently the LSPR feature of the Cu_7S_4@Pd heteronanostructures is mainly attributed to the Cu_7S_4 domain. As for the Cu_7S_4@Pd heteronanostructures, there is an apparent electrical field enhancement by all three wavelengths. In addition, the electrical field intensity for 1500 nm irradiation appears far stronger than 808 and 980 nm, indicating the overall LSPR of the heteronanostructure is more obvious if irradiation wavelength is close to the Cu_7S_4 LSPR peak. In addition, enhanced LSPR feature around the Pd domain was observed, which may be attributed to the extended influence from semiconductor domain to noble metal domain across the interface. This result, together with our previous observation (Figure 2a), suggests a promising pathway to effectively expand the localized electrical field enhancement from Cu_7S_4 to the whole Cu_7S_4@Pd heteronanostructure and offers potential to couple Cu_7S_4 with other metal catalysts without strong LSPR features.

To assess catalytic activity of Cu_7S_4@Pd, Suzuki coupling reaction between iodobenzene and phenylboronic acid was used as the model reaction. The hydrophobic Cu_7S_4@Pd nanoparticles were dispersed into water with the help of cetyltrimethylammonium bromide (CTAB) (TEM image is shown in Supporting Information Figure S6). Given that 1500 nm diode laser is close to Cu_7S_4@Pd LSPR peak position, here we applied 1500 nm laser as illumination source in our trials. The concentration of the catalyst stock solution was quantified by inductively coupled plasma mass spectrometry (ICP-MS), and the dosage was carefully calculated prior to each test (Supporting Information Table S2). Initially, control experiments were carried out without laser irradiation nor heating. No traceable product was detected. Moreover, since our photocatalytic system is based on LSPR enhancement effect, photon utilization efficiency is determined dominantly by resonance frequency of Cu_7S_4@Pd heteronanostructure. Irradiation source frequency at or close to intrinsic plasmon frequency on Cu_7S_4@Pd heteronanostructure would benefit catalytic activity most. To verify this effect, we applied 808, 980, and 1500 nm irradiation light for the Suzuki coupling reaction. The photocatalytic activities obtained in 1500 nm trial were much higher than those of 808 or 980 nm trials at all three reaction time intervals (10, 20, and 30 min). For example, with reaction time of 30 min, 1500 nm irradiation gave a 97% conversion (Figure 3a and Figure 3c1), while 808 nm resulted in 45% conversion and 980 nm yielded slightly higher than 50% conversion (Figure 3a). When phenylboronic acid was replaced with *p*-tolylboronic acid, we also observed similar trend (Figure 3b).

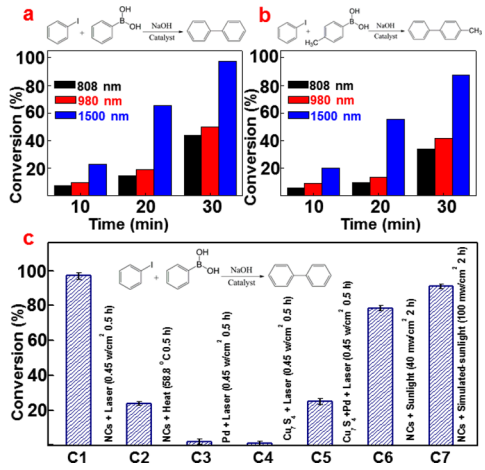

Figure 3. Photocatalytic activity of Cu_7S_4@Pd nanostructure for Suzuki coupling reactions of iodobenzene with different reagents: (a) phenylboronic acid and (b) *p*-tolylboronic acid. Both reactions were under 808, 980, and 1500 nm laser irradiation for 30 min. The power density of each laser source is 0.45 W/cm^2. (c) Conversion comparison with different catalysts under various catalytic conditions. All lasers used here is the 1500 nm laser.

It is generally recognized that extensive LSPR features can give rise to photocatalysis and photothermal effect simultaneously.[10,54] In order to evaluate influence of these two effects, we used conventional heating as comparison tests. We began to record temperature changes with 1500 nm laser irradiation (0.45 W/cm^2) and found the temperature raised and kept at 58.8 °C within 5 min (Supporting Information Figure S7). Thus, we ran the reaction with Cu_7S_4@Pd heteronanostructures at 58.8 °C for 30 min in dark environment (Figure 3c2). Less than 25% conversion was recorded. This is substantially different from nearly 100% conversion provided by laser irradiation from which we can conclude that photothermal effect only contributes to part of the catalytic effect, while

DOI: 10.1021/acs.nanolett.5b00950
Nano Lett. 2015, 15, 6295−6301

photocatalysis serves as prevailing factor to determine overall activity.

Additionally, to prove the synergetic effect of Cu_7S_4 and Pd nanostructures as an integrated system we conducted reactions based on Pd nanoparticles alone, Cu_7S_4 nanoparticles alone, and physical mixture of the two (no chemical bonding between two components like in Cu_7S_4@Pd). It can be seen in Figure 3c3,c4 that neither Pd-only trial nor Cu_7S_4-only trial exhibited yield higher than 10%. These results can be interpreted as follows: the Pd domain has little contribution to the NIR LSPR effects, and Cu_7S_4 alone has limited catalytic effect in the Suzuki coupling reaction. The mixture of these two components achieved ~32% conversion (Figure 3c5), which is far lower than that from Cu_7S_4@Pd (nearly 100% converted). This is a strong proof that intimate vicinity between Cu_7S_4 and Pd domains is crucial, and the photocatalysis is a synergetic outcome of integrated Cu_7S_4 and Pd components.

To evaluate the effectiveness of the Cu_7S_4@Pd heteronanostructures in other reactions, we further assessed them in the selective oxidation of benzyl alcohol and the hydrogenation of nitrobenzene. First we examined the plasmon enhancement effect on these two reactions through wavelength dependent studies. Sources of 808, 980, and 1500 nm were used. In both oxidation and hydrogenation reaction trials, 1500 nm trials demonstrated best conversions, followed by 980 nm, and then the 808 nm (Figure 4a,b). Similar to wavelength-dependent results obtained in the Suzuki coupling reaction, these results clearly show the plasmon resonance enhancement near the LSPR peak exhibits predominant influence in photocatalytic process. Again, the photothermal effect still serves as minor effect compared to that of photocatalysis. In oxidation reaction, direct heating the reaction solution at 58.8 °C gave conversion of less than 30% and in reduction reaction the conversion under identical conventional heating condition was 22% (Figure 4c,d). Neither of them is comparable to near 100% conversion obtained under 1500 nm irradiation (Figure 4c,d). In addition, we used pure Pd and Cu_7S_4 to conduct control experiments. In both oxidation and reduction reactions, Pd or Cu_7S_4 nanocatalysts yielded less than 10% conversion with 1500 nm irradiation (Figure 4c,d). Moreover, we found that in the benzyl alcohol oxidation reaction products, that is, benzaldehyde, benzyl benzoate, and benzoic acid (Figure 4e), 1500 nm source yielded 99.57% selectivity toward benzaldehyde, while 808 and 980 nm gave 95.87% and 93.43% selectivity, respectively. The selectivity toward benzyl benzoate also changes significantly with respect to wavelengths. The selectivity of 3.90% was obtained for 808 nm trial, 5.62% for 980 nm trial, and merely 0.28% for 1500 nm trial.

We further carried out the catalytic reaction with simulated sunlight source to examine the pragmatic feasibility of our photocatalyst. After being exposed to the simulated sunlight (100 mW/cm^2) for 2 h, nearly 96% conversion was observed for Suzuki coupling reaction (Figure 3c7). Inspired by this promising result, we also conducted the solar photocatalysis reaction with real sunlight. Under the typical solar irradiation in local outdoor environment (the average solar power density was 40 mW/cm^2), 78.6% iodobenzene was converted to biphenyl after 2 h exposure (Figure 3c6). In benzyl alcohol oxidation reaction, 77.8% conversion was obtained (the average solar power density was 42 mW/cm^2), and ~97% conversion in nitrobenzene hydrogenation was achieved with average solar power density of 37 mW/cm^2 (Figure 4c,d). In addition, the recyclability tests based on Suzuki coupling reaction revealed

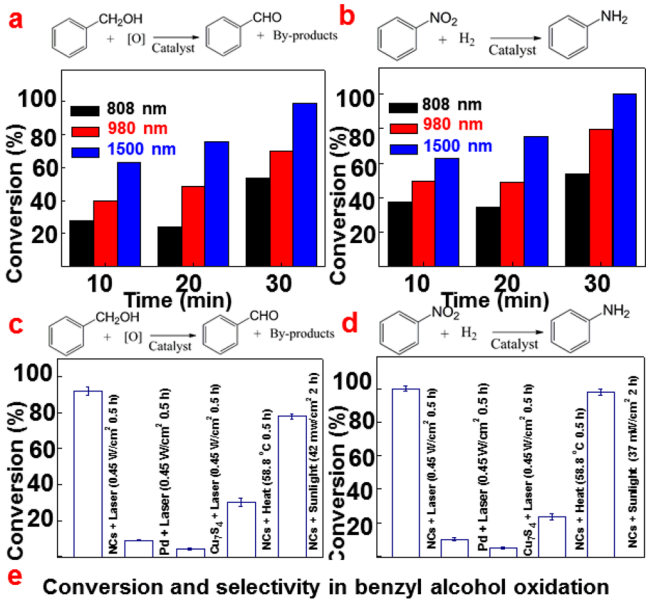

e Conversion and selectivity in benzyl alcohol oxidation

Wavelength (nm)	Conversion (%)	Selectivity (%)		
		Benzaldehyde	*Benzyl benzoate*	*Benzoic acid*
808	53.63	95.87	3.90	0.23
980	69.75	93.43	5.62	0.95
1500	99.72	99.57	0.28	0.15

Figure 4. Photocatalytic activities of Cu_7S_4@Pd in (a) selective oxidation of benzyl alcohol and (b) hydrogenation of nitrobenzene under 808, 980, and 1500 nm irradiation. The power density for three wavelength lasers is 0.45 W/cm^2. (c) Conversion comparison of different catalysts under different catalytic conditions in selective oxidation of benzyl alcohol. (d) Conversion comparison of different catalysts under different catalytic conditions in reduction of nitrobenzene. (e) Products selectivity profile in selective oxidation of benzyl alcohol using different irradiation wavelengths.

that the photocatalytic efficiency and catalyst morphology preserved after five cycles, which is desirable with respect to economical consideration (Supporting Information Figure S8). Lastly, because our synthetic protocol can be extended to Cu_7S_4@Pt, Cu_7S_4@Au, and Cu_7S_4@Ag, we assessed their catalytic performances through oxidation and reduction reactions under sunlight for 2 h (the average solar power density was 47.5 mW/cm^2). Our results indicated they all display fairly good catalytic activities (Supporting Information Figure S9).

In order to explain the photocatalytic enhancement mechanism, we measured band structure of Cu_7S_4. The indirect and direct band gap of Cu_7S_4 was determined by Kubelka–Munk method[62] as 0.821 and 1.432 eV, respectively (Figure 5a,b). Valence band position was detected via electrochemical method[62] and calculated as −5.316 eV (Figure 5c,d). Furthermore, the gap between the top of valence band and Fermi level of Cu_7S_4 is estimated to be 0.125 eV (see Supporting Information for calculation), that is, the Fermi level of Cu_7S_4 (E_F = −5.191 eV) is above and close to its valence band, representing a typical p-type semiconductor (Figure 5e).[58] As the experimental results suggest that reactions illuminated by 1500 nm (~0.826 eV, close to LSRP peak) show far higher conversion rate than those by 808 nm (1.534 eV) and 980 nm (1.265 eV), it is unlikely that the interband

DOI: 10.1021/acs.nanolett.5b00950
Nano Lett. 2015, 15, 6295–6301

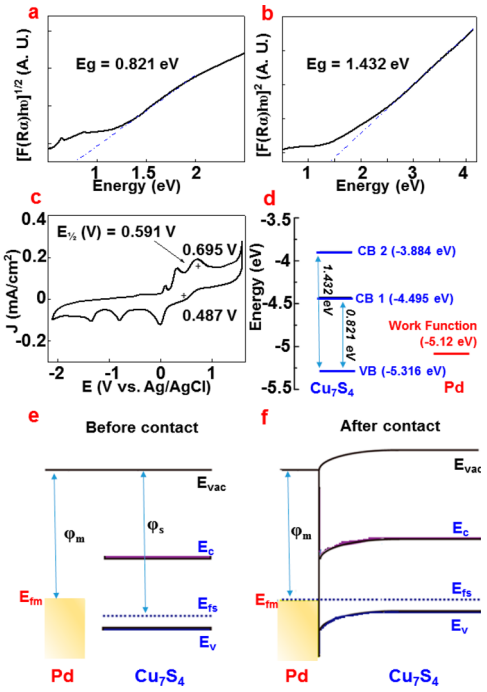

Figure 5. Plots of the indirect (a) and direct (b) band gap of Cu_7S_4. (c) The cyclic voltammograms of Cu_7S_4. (d) The energy level line-up of Cu_7S_4. (e,f) Energy band diagram of metal (Pd) and p-type semiconductor (Cu_7S_4) before (e) and after (f) contact. E_g: band gap. E_{vac}: vacuum energy. E_c: conduction band position. E_v: valence band position. φ_m: metal work function. φ_s: semiconductor work function. E_{fm}: metal Fermi level. E_{fs}: semiconductor Fermi level.

transition has major effect on the catalytic reactions. We suggest that under 1500 nm illumination, LSRP absorption of Cu_7S_4 generates "hot holes", which possess sufficient energy to overcome the small Schottky barrier and inject into Pd domain. It is possible the hot-hole injection renders the Pd surface electron-deficient, which then serves as a key contribution to the observed photocatalytic enhancement effect for Cu_7S_4@Pd. This hypothesis matches reasonably well with our experimental results. In terms of Suzuki coupling reaction, theoretical studies indicated that the rate-limiting step is the oxidative addition of aryl halides onto Pd(0).[63] This process favors the positively charged Pd surface, which resembles electron-withdrawing ligands and can promote activation of aryl halides.[63] In the catalytic oxidation of benzyl alcohol, hot holes injected to Pd domain might function like oxidant and react in situ with benzyl alcohol and the derivative species adsorbed on Pd surface, so as to accelerate the reaction. In the hydrogenation reaction, Pd is generally considered active catalyst but suffers from rapid surface-poisoning due to strong binding of H atoms.[64,65] Previous studies suggested negative charges enhanced the binding of H atoms on Pd surface, while positive charges help with dissociation of adsorbed H atoms.[64] Hence, we propose the transferred hot holes can facilitate hydrogenation reaction through promoting H atom dissociation and thus keep Pd surface consistently active, leading to enhanced catalyst activity.

In conclusion, we have developed a facile strategy for the synthesis of Cu_7S_4@Pd heteronanostructures with excellent NIR LSPR properties and photocatalytic activities. This synthetic method can be easily extended to other semiconductor–metal heteronanostructures. The Cu_7S_4 semiconductor domain acts as a plasmonic component for efficient photoharvesting in NIR region, while the Pd noble metal domain provides active sites for organic reactions. Experiment results indicate Cu_7S_4 and Pd domains function as a synergetic system. Upon 1500 nm irritation and LSPR absorption, hot-holes can be generated on Cu_7S_4, which can inject into Pd domain to render hole-rich Pd surface. This hole-rich Pd surface may serve as effective catalytic sites for Suzuki coupling, oxidation, and reduction reactions. Furthermore, unlike most of the traditional semiconductor–metal hybrid photocatalysts in which the LSPR of the noble metal nanoparticles assist the visible range absorption of the semiconductor, here Cu_7S_4 nanoparticle utilizes NIR range photon through LSPR and extends the benefits to the metal catalyst. This leads to exciting potentials in photocatalysis especially considering that Cu_7S_4 has been reported to demonstrate tunable LSPR at different carrier densities.[52] Although the exact mechanism and the synergetic roles of Cu_7S_4 and Pd in these photocatalytic reactions need further investigations, this study opens up wide possibilities in utilizing NIR LSPR properties of copper chalcogenides to enhance photocatalysis. Furthermore, incorporation of various metal nanocatalysts with Cu_7S_4 is expected to broaden materials choice and hence exhibit more fascinating catalytic performances.

■ ASSOCIATED CONTENT

Supporting Information

The Supporting Information is available free of charge on the ACS Publications website at DOI: 10.1021/acs.nanolett.5b00950.

Detailed experimental procedures, equipment list, simulation setup, and theoretical calculation steps; TEM images of Cu_7S_4 and Pd nanoparticles (Figure S1); standard XRD peak locations of $Cu_{2-x}S$ (Table S1); TEM, HRTEM images and respective XRD patterns of Cu_7S_4@Au, Cu_7S_4@Pt, and Cu_7S_4@Ag heteronanostructures (Figures S2 and 3); FDTD simulation results for Pd and Cu_7S_4 nanoparticle with different irradiation wavelengths (Figures S4 and S5); TEM images of Cu_7S_4@Pd heteronanostructures in aqueous solution (Figure S6); the catalyst dosage applied in reactions (Table S2); reaction solution temperature change with respect to time under irradiation of different wavelengths (Figure S7); the recyclability test result and TEM image of Cu_7S_4@Pd after reactions (Figurew S8); the photocatalytic performance of Cu_7S_4@Pt, Cu_7S_4@Au and Cu_7S_4@Ag (Figure S9).
(PDF)

■ AUTHOR INFORMATION

Corresponding Authors

*E-mail: lywang@mail.buct.edu.cn (L.W.).
*E-mail: yhuang@seas.ucla.edu (Y.H.).

Author Contributions

J.C. and Y.L. contributed equally to the manuscript.

All authors contributed to the preparation of this manuscript. L.W. conceived the idea. J.C., L.C., J.X., J.M., G.F., and L.W. performed experiments, data collection, analysis, and explanation. L.L. and L.Z. helped with simulation. Y.L., E.Z., H.W., and Y. H. helped with design of the experiments, data analysis, and organization of manuscript. All authors have given approval to the final version.

DOI: 10.1021/acs.nanolett.5b00950
Nano Lett. 2015, 15, 6295–6301

Notes

The authors declare no competing financial interest.

■ ACKNOWLEDGMENTS

The authors gratefully acknowledge the financial support by the National Natural Science Foundation of China (21475007 and 21275015), the State Key Project of Fundamental Research of China (2011CB932403). L.W. acknowledges the support from the "Innovation and Promotion Project of Beijing University of Chemical Technology" and the "Public Hatching Platform for Recruited Talents of Beijing University of Chemical Technology". Y.H. acknowledges support from ARO through Award No. 54709-MS-PCS.

■ REFERENCES

(1) Navalon, S.; de Miguel, M.; Martin, R.; Alvaro, M.; Garcia, H. *J. Am. Chem. Soc.* **2011**, *133*, 2218−2226.
(2) Eley, C.; Li, T.; Liao, F. L.; Fairclough, S. M.; Smith, J. M.; Smith, G.; Tsang, S. C. E. *Angew. Chem., Int. Ed.* **2014**, *53*, 7838−7842.
(3) Li, P.; Wei, Z.; Wu, T.; Peng, Q.; Li, Y. D. *J. Am. Chem. Soc.* **2011**, *133*, 5660−5663.
(4) Attia, Y. A.; Buceta, D.; Blanco-Varela, C.; Mohamed, M. B.; Barone, G.; López-Quintela, M. A. *J. Am. Chem. Soc.* **2014**, *136*, 1182−1185.
(5) Zheng, Z. K.; Tachikawa, T.; Majima, T. *J. Am. Chem. Soc.* **2014**, *136*, 6870−6873.
(6) Yu, X. L.; Shavel, A.; An, X. Q.; Luo, Z. S.; Ibanez, M.; Cabot, A. *J. Am. Chem. Soc.* **2014**, *136*, 9236−9239.
(7) Zhang, S.; Metin, O.; Su, D.; Sun, S. H. *Angew. Chem., Int. Ed.* **2013**, *52*, 3681−3684.
(8) Choi, C.; Feng, J.; Li, Y. G.; Wu, J.; Zak, A.; Tenne, R.; Dai, H. J. *Nano Res.* **2013**, *6*, 921−928.
(9) Yahaya, A. H.; Gondal, M. A.; Hameed, A. *Chem. Phys. Lett.* **2004**, *400*, 206−212.
(10) Huang, X. Q.; Li, Y. J.; Chen, Y.; Zhou, H. L.; Duan, X. F.; Huang, Y. *Angew. Chem., Int. Ed.* **2013**, *52*, 6063−6067.
(11) Huang, X. Q.; Li, Y. J.; Chen, Y.; Zhou, E. B.; Xu, Y. X.; Zhou, H. L.; Duan, X. F.; Huang, Y. *Angew. Chem., Int. Ed.* **2013**, *52*, 2520−2524.
(12) Huang, X. Q.; Zhu, E. B.; Chen, Y.; Li, Y. J.; Chiu, C. Y.; Xu, Y. X.; Lin, Z. Y.; Duan, X. F.; Huang, Y. *Adv. Mater.* **2013**, *25*, 2974−2979.
(13) Huang, X. Q.; Tang, S. H.; Mu, X. L.; Dai, Y.; Chen, G. X.; Zhou, Z. Y.; Ruan, F. X.; Yang, Z. L.; Zheng, N. F. *Nat. Nanotechnol.* **2011**, *6*, 28−32.
(14) Zhang, H.; Jin, M. S.; Wang, J. G.; Li, W. Y.; Camargo, P. H. C.; Kim, M. J.; Yang, D. R.; Xie, Z. X.; Xia, Y. A. *J. Am. Chem. Soc.* **2011**, *133*, 6078−6089.
(15) Xia, X. H.; Figueroa-Cosme, L.; Tao, J.; Peng, H. C.; Niu, G. D.; Zhu, Y. M.; Xia, Y. N. *J. Am. Chem. Soc.* **2014**, *136*, 10878−10881.
(16) Chiu, C. Y.; Li, Y. J.; Ruan, L. Y.; Ye, X. C.; Murray, C. B.; Huang, Y. *Nat. Chem.* **2011**, *3*, 393−399.
(17) Jia, Y. Y.; Jiang, Y. Q.; Zhang, J. W.; Zhang, L.; Chen, Q. L.; Xie, Z. X.; Zheng, L. S. *J. Am. Chem. Soc.* **2014**, *136*, 3748−3751.
(18) Wu, Y. E.; Wang, D. S.; Niu, Z. Q.; Chen, P. C.; Zhou, G.; Li, Y. D. *Angew. Chem., Int. Ed.* **2012**, *51*, 12524−12528.
(19) Li, L. L.; Chen, X. B.; Wu, Y. E.; Wang, D. S.; Peng, Q.; Zhou, G.; Li, Y. D. *Angew. Chem., Int. Ed.* **2013**, *52*, 11049−11053.
(20) Xie, S. F.; Zhang, H.; Lu, N.; Jin, M. S.; Wang, J. G.; Kim, M. J.; Xie, Z. X.; Xia, Y. N. *Nano Lett.* **2013**, *13*, 6262−6268.
(21) Hong, X.; Wang, D. S.; Cai, S. F.; Rong, H. P.; Li, Y. D. *J. Am. Chem. Soc.* **2012**, *134*, 18165−18168.
(22) Chen, C.; Kang, Y. J.; Huo, Z. Y.; Zhu, Z. W.; Huang, W. Y.; Xin, H. L. L.; Snyder, J. D.; Li, D. G.; Herron, J. A.; Mavrikakis, M.; Chi, M. F.; More, K. L.; Li, Y. D.; Markovic, N. M.; Somorjai, G. A.; Yang, P. D.; Stamenkovic, V. R. *Science* **2014**, *343*, 1339−1343.
(23) Xie, S. F.; Lu, N.; Xie, Z. X.; Wang, J. G.; Kim, M. J.; Xia, Y. N. *Angew. Chem., Int. Ed.* **2012**, *51*, 10266−10270.
(24) Blankenship, R. E.; Tiede, D. M.; Barber, J.; Brudvig, G. W.; Fleming, G.; Ghirardi, M.; Gunner, M. R.; Junge, W.; Kramer, D. M.; Melis, A.; Moore, T. A.; Moser, C. C.; Nocera, D. G.; Nozik, A. J.; Ort, D. R.; Parson, W. W.; Prince, R. C.; Sayre, R. T. *Science* **2011**, *332*, 805−809.
(25) Linic, S.; Christopher, P.; Ingram, D. B. *Nat. Mater.* **2011**, *10*, 911−921.
(26) Christopher, P.; Xin, H. L.; Linic, S. *Nat. Chem.* **2011**, *3*, 467−472.
(27) Wang, F.; Li, C. H.; Chen, H. J.; Jiang, R. B.; Sun, L. D.; Li, Q.; Wang, J. F.; Yu, J. C.; Yan, C. H. *J. Am. Chem. Soc.* **2013**, *135*, 5588−5601.
(28) Gao, H. W.; Liu, C.; Jeong, H. E.; Yang, P. D. *ACS Nano* **2012**, *6*, 234−240.
(29) Zhang, T. T.; Zhao, H. Y.; He, S. N.; Liu, K.; Liu, H. Y.; Yin, Y. D.; Gao, C. B. *ACS Nano* **2014**, *8*, 7297−7304.
(30) Zedan, A. F.; Moussa, S.; Terner, J.; Atkinson, G.; El-Shall, M. S. *ACS Nano* **2013**, *7*, 627−636.
(31) Xia, Y. N.; Li, W. Y.; Cobley, C. M.; Chen, J. Y.; Xia, X. H.; Zhang, Q.; Yang, M. X.; Cho, E. C.; Brown, P. K. *Acc. Chem. Res.* **2011**, *44*, 914−924.
(32) Dasgupta, N. P.; Liu, C.; Andrews, S.; Prinz, F. B.; Yang, P. D. *J. Am. Chem. Soc.* **2013**, *135*, 12932−12935.
(33) Zhang, H.; Li, Y. J.; Ivanov, I. A.; Qu, Y. Q.; Huang, Y.; Duan, X. F. *Angew. Chem., Int. Ed.* **2010**, *49*, 2865−2868.
(34) Tu, N. N.; Wang, L. Y. *Chem. Commun.* **2013**, *49*, 6319−6321.
(35) Bardhan, R.; Lal, S.; Joshi, A.; Halas, N. J. *Acc. Chem. Res.* **2011**, *44*, 936−946.
(36) Jain, P. K.; Huang, X. H.; El-Sayed, I. H.; El-Sayed, M. A. *Acc. Chem. Res.* **2008**, *41*, 1578−1586.
(37) Primo, A.; Marino, T.; Corma, A.; Molinari, R.; Garcia, H. *J. Am. Chem. Soc.* **2011**, *133*, 6930−6933.
(38) Zahran, E. M.; Bedford, N. M.; Nguyen, M. A.; Chang, Y. J.; Guiton, B. S.; Naik, R. R.; Bachas, L. G.; Knecht, M. R. *J. Am. Chem. Soc.* **2014**, *136*, 32−35.
(39) Long, R.; Prezhdo, O. V. *J. Am. Chem. Soc.* **2014**, *136*, 4343−4354.
(40) Yamada, Y.; Tsung, C. K.; Huang, W.; Huo, Z. Y.; Habas, S. E.; Soejima, T.; Aliaga, C. E.; Somorjai, G. A.; Yang, P. D. *Nat. Chem.* **2011**, *3*, 372−376.
(41) Wu, K. F.; Zhu, H. M.; Liu, Z.; Rodriguez-Cordoba, W.; Lian, T. Q. *J. Am. Chem. Soc.* **2012**, *134*, 10337−10340.
(42) He, W. W.; Kim, H. K.; Warner, W. G.; Melka, D.; Callahan, J. H.; Yin, J. J. *J. Am. Chem. Soc.* **2014**, *136*, 750−757.
(43) Kuo, C. H.; Yang, Y. C.; Gwo, S.; Huang, M. H. *J. Am. Chem. Soc.* **2011**, *133*, 1052−1057.
(44) Cho, S.; Lee, M. J.; Kim, M. S.; Lee, S.; Kim, Y. K.; Lee, D. H.; Lee, C. W.; Cho, K. H.; Chung, J. H. *J. Dermatol. Sci.* **2008**, *50*, 123−133.
(45) Tian, Q. W.; Hu, J. Q.; Zhu, Y. H.; Zou, R. J.; Chen, Z. G.; Yang, S. P.; Li, R. W.; Su, Q. Q.; Han, Y.; Liu, X. G. *J. Am. Chem. Soc.* **2013**, *135*, 8571−8577.
(46) Hsu, S. W.; On, K.; Tao, A. R. *J. Am. Chem. Soc.* **2011**, *133*, 19072−19075.
(47) Han, W.; Yi, L. X.; Zhao, N.; Tang, A. W.; Gao, M. Y.; Tang, Z. Y. *J. Am. Chem. Soc.* **2008**, *130*, 13152−13161.
(48) Han, S. K.; Gong, M.; Yao, H. B.; Wang, Z. M.; Yu, S. H. *Angew. Chem., Int. Ed.* **2012**, *51*, 6365−6368.
(49) Ding, X.; Liow, C. H.; Zhang, M.; Huang, R.; Li, C.; Shen, H.; Liu, M.; Zou, Y.; Gao, N.; Zhang, Z.; Li, Y.; Wang, Q.; Li, S.; Jiang, J. *J. Am. Chem. Soc.* **2014**, *136*, 15684−93.
(50) Cui, J. B.; Jiang, R.; Xu, S. Y.; Hu, G. F.; Wang, L. Y. *Small* **2015**, *11* (33), 4183−4190.
(51) Subramanian, V.; Wolf, E. E.; Kamat, P. V. *J. Am. Chem. Soc.* **2004**, *126*, 4943−4950.
(52) Luther, J. M.; Jain, P. K.; Ewers, T.; Alivisatos, A. P. *Nat. Mater.* **2011**, *10*, 361−366.

DOI: 10.1021/acs.nanolett.5b00950
Nano Lett. 2015, 15, 6295−6301

(53) Shaviv, E.; Schubert, O.; Alves-Santos, M.; Goldoni, G.; Di Felice, R.; Vallee, F.; Del Fatti, N.; Banin, U.; Sonnichsen, C. *ACS Nano* **2011**, *5*, 4712−4719.
(54) Banin, U.; Ben-Shahar, Y.; Vinokurov, K. *Chem. Mater.* **2014**, *26*, 97−110.
(55) Toshima, N.; Yonezawa, T. *New J. Chem.* **1998**, *22*, 1179−1201.
(56) Kim, S. M.; Lee, S. J.; Kim, S. H.; Kwon, S.; Yee, K. J.; Song, H.; Somorjai, G. A.; Park, J. Y. *Nano Lett.* **2013**, *13*, 1352−1358.
(57) Kriegel, I.; Rodriguez-Fernandez, J.; Da Como, E.; Lutich, A. A.; Szeifert, J. M.; Feldmann, J. *Chem. Mater.* **2011**, *23*, 1830−1834.
(58) Wang, S.; Riedinger, A.; Li, H.; Fu, C.; Liu, H.; Li, L.; Liu, T.; Tan, L.; Barthel, M. J.; Pugliese, G.; De Donato, F.; D'Abbusco, M. S.; Meng, X.; Manna, L.; Meng, H.; Pellegrino, T. *ACS Nano* **2015**, *9*, 1788−1800.
(59) Mukherjee, S.; Libisch, F.; Large, N.; Neumann, O.; Brown, L. V.; Cheng, J.; Lassiter, J. B.; Carter, E. A.; Nordlander, P.; Halas, N. J. *Nano Lett.* **2013**, *13*, 240−247.
(60) Li, J. T.; Cushing, S. K.; Bright, J.; Meng, F. K.; Senty, T. R.; Zheng, P.; Bristow, A. D.; Wu, N. Q. *ACS Catal.* **2013**, *3*, 47−51.
(61) Simon, T.; Bouchonville, N.; Berr, M. J.; Vaneski, A.; Adrovic, A.; Volbers, D.; Wyrwich, R.; Doblinger, M.; Susha, A. S.; Rogach, A. L.; Jackel, F.; Stolarczyk, J. K.; Feldmann, J. *Nat. Mater.* **2014**, *13*, 1013−1018.
(62) Kim, Y.; Park, K. Y.; Jang, D. M.; Song, Y. M.; Kim, H. S.; Cho, Y. J.; Myung, Y.; Park, J. *J. Phys. Chem. C* **2010**, *114*, 22141−22146.
(63) Miyaura, N.; Suzuki, A. *Chem. Rev.* **1995**, *95*, 2457−2483.
(64) Long, R.; Rao, Z. L.; Mao, K. K.; Li, Y.; Zhang, C.; Liu, Q. L.; Wang, C. M.; Li, Z. Y.; Wu, X. J.; Xiong, Y. J. *Angew. Chem., Int. Ed.* **2015**, *54*, 2425−2430.
(65) Bai, S.; Jiang, J.; Zhang, Q.; Xiong, Y. J. *Chem. Soc. Rev.* **2015**, *44*, 2893−2939.

DOI: 10.1021/acs.nanolett.5b00950
Nano Lett. 2015, 15, 6295−6301